Applied Geochemistry 172 (2024) 106105

Contents lists available at ScienceDirect

Applied Geochemistry

journal homepage: www.elsevier.com/locate/apgeochem

Interaction of aluminum alloys with MKPC and Portland-based cements on the metal-matrix interface

C. Fernández-García [a,*], P. Padilla-Encinas [b], R. Fernández [b], M.C. Alonso [a]

[a] Institute of Construction Science "Eduardo Torroja" (IETcc), CSIC, Serrano Galvache 4, 28033, Madrid, Spain
[b] Department of Geology and Geochemistry, Faculty of Sciences, Universidad Autónoma de Madrid, 28049, Madrid, Spain

ARTICLE INFO

Editorial Handling by: Erich Wieland

Keywords:
Metal LL-ILRW reactivity
Aluminium immobilisation
Cement interaction
Hydrogen release
Metal/matrix interface

ABSTRACT

Cementitious matrices are considered for the immobilisation of radioactive aluminium. The processes occurring at the interface between both materials are relevant for the long-term stability of the repository. The present study compares Ordinary Portland cement (OPC), CEM I-type, with alternative Portland blended cement (CEM IV and CEM I + 50% silica fume) and magnesium potassium phosphate cement (MKPC). Al A1050 and Al AA5754, with 3.5% Mg, have been used as reactive metal alloys. Two exposure conditions were employed: (1) water immersion and (2) isolated in sealed plastic films. Long-term corrosion monitoring (E_{corr}, i_{corr} and V_{corr}) was evaluated to understand the effect of Al reactivity in the matrix. The associated H_2 release was quantified to understand the changes at the metal/matrix interface. Furthermore, pore ion concentrations and the pore microstructure were evaluated. The metal/matrix interface alterations were analysed at the end of the tests. The study revealed that after 300 days of water immersion, the CEM I + 50% of silica fume matrix had reduced the pore solution pH down to 10.5 compared to CEM I, which remained high alkaline (pH 12.9), and CEM IV with no significant decreases (pH 12.3). In contrast, MKPC showed the lowest pH (7–9.8). Low Al corrosion rates were found with MKPC, followed by CEM I + 50% SF according to their lower pH. A corrosion product layer of 90-50 μm thickness was observed at the Al/CEM I matrix interface constituted of aluminium and oxygen. Furthermore, enrichment in Al was detected in the matrix (around 1 mm depth), causing the formation of ettringite nodules. Voids were detected at the interface level associated with the high volume of H_2 released. The MKPC matrix showed no alteration at the metal/matrix interface due to the lower reactivity of the matrix and lower H_2 release. A homogeneous and dense region (30 μm) rich in phosphorous, potassium and magnesium was observed near the metal surface.

1. Introduction

Low to intermediate-level radioactive wastes (LL-ILRW), including organic and inorganic solid and liquid forms, from the operation of nuclear power plants, fuel reprocessing, and other industrial activities require to undergo conditioning for correct storage and disposal to prevent unsuitable radioactive releases into the environment (Kónya and Nagy, 2018). The level of treatment is chosen depending on the waste characteristics. LL-IL metallic waste (e.g., aluminium, beryllium, Magnox …) must be immobilised before final disposal in a near-surface geological repository (Krall et al., 2022; Won et al., 1997). A physical system of engineered barriers is commonly used, including steel drums or concrete cells filled with a cementitious material for waste immobilisation (Deshwal and Panjagari, 2020; Paraskevoulakos et al., 2019). Ordinary Portland cement (OPC) type CEM I is usually considered as an immobilisation matrix; however, the high pH of its pore solution (up to 13.7) suggests limitations for immobilising some reactive waste metals. Al metal reacts in air or water, developing a protective and amphoteric alumina oxide layer (Al_2O_3) that is stable in a pH range from 4 to 9 to reach the passive state (Pourbaix and Burbank, 1964). Outside this pH region, the natural Al_2O_3 oxide layer dissolves, promoting Al corrosion in aqueous media. The overall reaction is expressed in equation (1), according to Vargel (2020):

$$2Al + 6H_2O \rightarrow Al_2O_3{\cdot}3H_2O + 3H_2 \quad (1)$$

This metal/matrix interaction can lead to the formation of H_2 gas, giving volumetric changes in the matrix, which may compromise the structural integrity of the confinement system, resulting in a high risk of

* Corresponding author.
E-mail address: carla.fernandez@ietcc.csic.es (C. Fernández-García).

https://doi.org/10.1016/j.apgeochem.2024.106105
Received 15 February 2024; Received in revised form 9 July 2024; Accepted 18 July 2024
Available online 25 July 2024

explosion and compromising the efficacy of the waste-form (Collier et al., 2010; Gardner et al., 2021). To find a suitable cement matrix, it is necessary to quantify the H_2 release volume.

The H_2-released volumes reported in the literature are summarised in Table 1 for pure Al and Al–Mg alloys immobilised in different cement matrices. Electrochemical methods (linear polarisation resistance (LPR) and electrochemical impedance spectroscopy (EIS)) or chemical methods (gas chromatography (GC) and gas counter) were employed to quantify the volume of H_2 released. An overview of the volumes of H_2 released reveals a clear scattering of data between the different studies. Differences are related to the pH of the pore solution, the technique used to determine the H_2 release (chemical methods produce, in general, lower volumes than electrochemical methods at the same age) and the curing conditions. As shown in Table 1, alkaline cementitious materials generated higher levels of H_2, as the pore solution pH strongly affects the Al reactivity.

Changes in the pore ion composition and the hydration products of CEM I matrices or alterations in their pore network can cause problems in the integrity of the cemented waste-form, which are undesirable for the encapsulation of some radioactive metallic wastes such as aluminium (Hayes and Godfrey, 2007; Kinoshita et al., 2013). Therefore, the benefit of the use of blended Portland binders, such as CEM III instead of OPC type CEM I, improved the management of radionuclides as in the metallic Al due to the lower temperature rise during hydration and a more refined pore network (Rahman et al., 2014).

Lowering the pore solution pH of a cementitious material or reducing the major ions in the pore water (e.g., Na, K, Ca) is known to reduce the alkalinity of these cement matrices (Vollpracht et al., 2016). The Al reactivity can take advantage of this process since the corrosion of Al strongly increases at pH > 9. Therefore, varying the cement proportions or introducing different mineral additions (e.g., fly ash (FA), silica fume (SF) or blast furnace slag (BFS)) could change the physicochemical properties of the Portland cement matrices, in particular the pore solution pH (Pandey and Sharma, 2000; Sharma and Pandey, 1999). Previous studies considering alternative Portland blended cement for Al immobilisation (CEM I + FA, CEM I + BFS) (Kinoshita et al., 2013; Liu et al., 2023; Setiadi et al., 2006) found that the internal pH decreased by one unit concerning the alkaline CEM I system. CEM III, which contains BFS, was investigated by Mendibide et al. (2021), who found an increase in the ionic pore water content at the Al/matrix interface due to Al reactivity and a drop in the pore solution pH.

Other studies used alternative binders such as calcium sulfoaluminate cement (CSA), made by calcining natural materials (e.g., limestone, bauxite, or clay) with gypsum or anhydrite (Zhou et al., 2006). The hydration product was mainly ettringite ($3CaO–Al_2O_3–3CaSO_4–32H_2O$) with high ye'elimite and calcium sulfate contents, which reduced the Al corrosion by consuming the free water, lowering the internal pH (down to 10.1) also by a leaching process (Cau Dit Coumes et al., 2014). Calcium aluminate cement (CAC), with an internal pH of around 11.7, is another alternative cement route for aluminium waste immobilisation. Mineral additions such as FA or SF react with calcium aluminates hydrates, forming strätlingite instead of pure hydro-garnet in the composition, which reduces the pore solution pH from 12.2 to 11.4, as García Calvo et al. (2013) found. The use of CAC for Al immobilisation has been reported in the literature (Cau Dit Coumes et al., 2014; Kinoshita et al., 2013).

Magnesium silicate cement (MSH) is also being investigated for Al immobilisation. This cement is prepared with MgO, $MgCO_3$, and SF, which reduces the pore solution pH to around 10, thereby decreasing the H_2 production (Cau Dit Coumes et al., 2014). Similarly, calcium phosphate cements with a wollastonite-based brushite binder (BRU) (Cau Dit Coumes et al., 2014) have an almost neutral internal pH within the Al passive domain.

Magnesium potassium phosphate cement (MKPC) is considered a suitable alternative for the immobilisation of Al LL-ILRW (Cau Dit Coumes et al., 2014; Covill et al., 2011; Gardner et al., 2021; Ionascu et al., 2014). The chemical reaction between acid KH_2PO_4 and the base MgO results in magnesium potassium phosphate hexahydrate ($MgKPO_4–6H_2O$), or K-struvite, as a main reaction product.

Previous studies with MKPC showed that many factors can alter the physicochemical stability of the matrix, such as the magnesia-to-phosphate ratio (M/P ratio). Fernández-García et al. (2024) suggested that a high M/P molar ratio (2, 3) reduces the phosphate content in the pore solution and increases the pH, which is not recommended for Al immobilisation, in favour of higher matrix stability. Padilla-Encinas et al. (2024) also found an increase in the pore solution pH at high M/P molar ratios (2, 3, 4) regardless of the type of filler added.

Aluminium reactivity due to corrosion phenomena plays an essential role in the physicochemical changes at the metal/matrix interface for long-term immobilisation. Mendibide et al. (2021) and Caes et al. (2023) studied the Al interaction in CEM I and CEM III pastes and mortars immersed in alkaline solution and at 95% RH using scanning electron microscope (SEM) coupled with energy dispersive X-ray (EDX) spectroscopy analyses. They found that the matrix is enriched at the interface level with Al, and a thick aluminium and oxygen corrosion layer is formed on the metal surface. Setiadi et al. (2006) studied the Al interaction with a CEM I + BFS cement at 95% RH via SEM and found a porous transition zone near the interface due to H_2 release.

Depending on the type of matrix used for immobilisation, the reactivity of Al can cause physicochemical changes in terms of stability at the interface in the metal/matrix interaction. The processes occurring at the interface are crucial for identifying Al-compatible cementitious materials for safe long-term immobilisation. The amount of H_2 gas produced by Al corrosion interacting with the matrix is a critical aspect to be assessed.

This paper focuses on characterising the changes that occur at the Al/matrix interface. The assessment of the H_2 evolution is carried out through electrochemical analyses due to the interaction of Al alloys (AA1050 and AA5754) with blended Portland cement (CEM IV and CEM I+50%SF) and MKPC as alternatives to OPC (CEM I). The physical changes at the interface (pore) were characterised by X-ray computed tomography (XCT) and SEM-EDX, affecting the matrix to understand the metal/matrix compatibility.

2. Materials and methods

2.1. Raw materials

To study the reactivity of aluminium, two alloys supplied by a Spanish producer were considered: (1) pure Al (A1050) and (2) Al–Mg alloy (AA5754), with 3.5% of Mg. The chemical composition of both alloys is summarised in Table 2.

Two types of cementitious composites based on calcium silicates were used: (1) ordinary Portland cement type CEM I 42.5R/SR (supplied by Cement Portland Valderrivas) with a particle size of 37.6 μm (d_{90}) and (2) two types of Portland cement mixed with mineral additions to control and reduce the pH through a pozzolanic reaction and consumption of portlandite. For this case, a commercial CEM IV/B 32.5N-SR (from LEMONA Cement S.A.) with a particle size of 32.7 μm (d_{90}) was used, which contains a 45–64% clinker and 36–55% FA. In addition, a CEM I 42.5R/SR blended with 50% SF (from FerroAtlántica S.A.) with a particle size of 2.3 μm (d_{90}) was also employed. The chemical compositions of the binders are summarised in Table 3.

MPKC was also employed, using a highly crystalline MgO (from Martin Marietta Specialities) with 97% purity and a particle size of 38.4 μm (d_{90}), whose chemical composition is given in Table 3. KH_2PO_4 (from Krista TM, 98% purity) and H_3BO_3 (from VWR Chemicals, ≥99.5% purity) as a setting retarder are also added. Volcanic ash (VA) produced from the eruption of the Cumbre Vieja volcano, La Palma, in 2021 (Padilla-Encinas et al., 2024) or low-CaO FA type F from a Spanish producer with a particle size of 170 μm (d_{90}) and a vitreous structure (Perona et al., 2023) were introduced as fillers to improve rheology

Table 1
Overview of H_2 gas released from pure Al and Al–Mg alloys using different cementitious materials and curing conditions: relative humidity (RH); isolated in sealed plastic or steel box/containers and immersed in water (Water Imm).

Cement system	Al alloy	Matrix	pH	Curing	Test	H_2 (L/m^2)	Days	Reference
CEM I	Pure Al	Mortar	12.5	Isolated (plastic box)	EIS	10.00	1	Delpech et al. (2017)
						70.00	7	
						150.00	50	
				Isolated (steel box)	GC	40.00	1	
				Water Imm	LPR	2.00	1	Perona et al. (2023)
						5.00	7	
		Paste	13	Isolated (steel box)	GC	40.00	1	Cau Dit Coumes et al. (2014)
			13.1	95%	Gas counter	90.00	1	Liu et al. (2023)
				RH		170.00	≈7	
			13			20.70	1	Kinoshita et al. (2013)
						145.00	7	
			12.9			50.00	1	Liu et al. (2023)
						140.00	≈7	
			12.3			20.00	1	
						50.00	≈7	
	Al + 3.5%Mg	Mortar	12.5	Water Imm	LPR	1.00	1	Perona et al. (2023)
						2.00	7	
		Paste	12.4	95%	Gas counter	24.00	1	Mendibide et al. (2021)
				RH		28.00	7	
						38.00	50	
CEM III/C			11.5			4.00	1	
						4.00	7	
						4.00	50	
MKPC 1M	Pure Al	Mortar	8	Isolated (plastic box)	EIS	0.10	1	Delpech et al. (2017)
						0.20	7	
						1.50	50	
				Isolated (steel box)	GC	0.20	1	
						0.30	7	
						0.40	50	
			7.2	Water Imm	LPR	0.01	1	Perona et al. (2023)
						0.05	7	
			8.6	100% RH		0.10	1	Fernández-García et al. (2024)
						0.41	7	
						1.20	50	
			7.8	Isolated (plastic box)		0.15	1	
						0.20	7	
						0.40	50	
			8	Isolated (steel box)	GC	0.04	1	Poras et al. (2023)
						0.12	7	
						0.16	50	
				Isolated (plastic box)	EIS	0.20	1	
						0.30	7	
						0.30	50	
		Paste	5.2	Isolated (steel box)	GC	0.10	1	Cau Dit Coumes et al. (2014)
						0.50	7	
						0.50	50	
	Al + 2% Mg	Mortar	8	Isolated (plastic box)	EIS	0.10	1	Poras et al. (2023)
						0.30	7	
						0.50	50	
				Isolated (steel box)	GC	0.02	1	
						0.12	7	
						0.18	50	
	Al + 3.5%Mg		7.2	Water Imm	LPR	0.04	1	Perona et al. (2023)
						0.33	7	
			8.6	100% RH		0.10	1	Fernández-García et al. (2024)
						0.40	7	
						1.40	50	
			7.8	Isolated (plastic box)		0.15	1	
						0.20	7	
						0.40	50	
	Al + 3% Mg		8	Isolated (steel box)	GC	0.04	1	Poras et al. (2023)
						0.12	7	
						0.24	50	
				Isolated (plastic box)	EIS	0.18	1	
						0.50	7	
						0.70	50	
	Al + 4% Mg			Isolated (steel box)	GC	0.01	1	
						0.08	7	
						0.14	50	
				Isolated (plastic box)	EIS	0.15	1	
						0.40	7	
						0.65	50	

(*continued on next page*)

Table 1 (*continued*)

Cement system	Al alloy	Matrix	pH	Curing	Test	H_2 (L/m^2)	Days	Reference
	Al + 4.5%Mg			Isolated (steel box)	GC	0.01	1	
						0.08	7	
						0.14	50	
				Isolated (plastic box)	EIS	0.01	1	
						0.30	7	
						0.50	50	
MKPC 2M	Pure Al	Mortar	10.3	100% RH	LPR	0.20	1	Fernández-García et al. (2024)
						1.40	7	
						3.60	50	
	Al + 3.5%Mg		10.3			0.40	1	
						2.20	7	
						4.60	50	
MKPC 3M	Pure Al		10.5			0.22	1	
						1.40	7	
						5.00	50	
	Al + 3.5%Mg		10.5			0.20	1	
						2.20	7	
						6.00	50	
CSA	Pure Al	Paste	10.1	Isolated (steel box)	GC	0.10	1	Cau Dit Coumes et al. (2014)
						5.00	7	
						7.00	50	
CAC			12.1	95% RH	Gas counter	1.40	1	Kinoshita et al. (2013)
						10.00	7	
			10.5	Isolated (steel box)	GC	1.00	1	Cau Dit Coumes et al. (2014)
						8.00	7	
			–			0.10	1	
						7.00	7	
MSH			10			0.10	1	
						3.00	7	
						35.00	50	
BRU			–			0.10	1	
						3.00	7	

Table 2
Chemical composition of pure Al (A1050) and Al–Mg alloy (AA5754) (wt. %).

Material	Al	Mg	Fe	Cu	Si	Mn	Cr	Zn	Ti
A1050	99.50	0.05	0.15	0.001	0.14	0.05	–	0.05	0.05
AA5754	94.50	3.50	0.40	0.30	0.40	0.30	0.25	0.20	0.15

Table 3
Chemical composition of OPC type CEM I, MKPC and Portland blended cement: binders and raw materials (in wt. %).

Material	Na_2O	K_2O	CaO	SiO_2	Al_2O_3	Fe_2O_3	MgO	SO_3	CaO_{free}
CEM I	0.18	0.34	60.30	17.40	4.68	5.08	1.78	3.17	1.85
CEM IV	0.57	1.44	41.46	32.63	12.90	4.49	1.61	3.45	–
SF	0.09	0.66	0.56	97.65	0.30	0.12	0.21	0.24	–
MgO	–	–	1.07	1.01	0.37	0.17	96.63	0.01	–
FA	–	–	4.78	42.44	26.95	18.40	0.80	1.44	–
VA	4.87	2.06	13.53	35.33	11.27	18.81	7.14	0.12	–

fluidity and reduce the temperature rise during the acid-base reaction and setting of the matrix. The compositions are listed in Table 3.

Table 4
Paste and mortar mix proportions for MKPC and Portland cement-based systems.

Material	System	M/P	H_2O/s	FA/s	Sand/s	H_3BO_3/s
		Molar ratio	Mass ratio			
MKPC	Mortar	1	0.51	1.00	1.00	0.02
	Paste	1	0.40	1.00	–	0.02
CEM I	Mortar	–	0.51	–	3.00	–
	Paste	–	0.40	–	–	–
CEM IV	Mortar	–	0.51	–	3.00	–
CEM I+50%SF	Mortar	–	0.51	–	3.00	–

2.2. Samples preparation: mortar and cement paste

Mortar and cement paste samples of CEM I, CEM IV, CEM I+50%SF and MKPC were prepared using the mix dosages listed in Table 4. The solid part in the matrix preparation corresponds with the cement proportion in CEM I, CEM IV and CEM I+50%SF systems or MgO + KH_2PO_4 in MKPC systems. A water/solid (w/s) mass ratio of 0.40 for pastes and 0.51 for mortars were employed. A 1M ratio of MgO/KH_2PO_4 (M/P) was used. Standardised graded sand with a 99% silica content (from SIBELCO minerals, particle size ≤2 mm) was used for the mortar preparation with a sand/solid ratio shown in Table 4. The samples were prepared according to the standard (Certificación, 1996): solids components were pre-mixed in a Turbula for 20–30 min. The homogenised powder was mixed with demineralised water (having pre-dissolved H_3BO_3 for the MKPC system) at low to high speed for 3 min while sand was added for mortar systems. The mortar or paste was then cast in the mould until hardening and demoulded after 24 h.

Two different curing conditions were used: 1) water immersion for mortars (Water Imm) and 2) isolated in sealed plastic films for cement pastes. All specimens were kept at a room temperature of 22 ± 2 °C. Table 5 summarises for each cement system the specimen geometry and the curing condition used according to the type of test performed:

- For the studies in cement pastes, cubes of 3 × 3 × 3 cm^3 having a coupon of pure Al (A1050) of 2 × 2 × 0.02 cm^3 embedded were prepared. The hardened samples were demoulded 24 h after mixing and wrapped in plastic films within a chamber set at a constant temperature for 4 months in the case of the CEM I matrix and up to 1 year for the MKPC matrix with volcanic ash as filler material. After curing, samples were used to study the physical Al/matrix interface using the XCT technique, as described later.
- For studies in mortars, cubes of 4 × 4 × 4 cm^3 of MKPC with the FA type F as filler and CEM I, CEM IV and CEM I + 50%SF were prepared with embedded coupons of 10 × 1.5 × 0.02 cm^3 of pure Al (A1050) and Al–Mg alloy (AA5754). The Al plate was first cleaned with isopropanol, and a 9 cm^2 exposure surface was delimited with isolating tape. Samples were demoulded 24 h after mixing and immersed in deionised water in individual containers for each type of cementitious matrix over 300 days without renewing the water. To avoid carbonation, the containers remained closed with a lid and were opened only at the time of analysis. After 300 days of water immersion, the samples were air-dried for 6 days to decrease the water in the pores of the mortar. The samples were painted with epoxy except for one face, and only CEM I and MKPC matrices were immersed in new deionised water for another 250 days. Other set of all matrices were immersed in alkaline water (results not considered in the present study). Mortar samples were devoted to monitoring Al corrosion after the first 24 h of hardening. The pore solution composition and internal pH of the mortar samples were characterised at different ages of the exposure period indicated in Table 5, described later.

2.3. Test methods

2.3.1. Corrosion monitoring of Al alloys

Electrochemical corrosion response was monitored on the coupons of pure Al (A1050) and Al–Mg alloy (AA5754) embedded in mortar samples. A three-electrode cell configuration was used (Fig. 1a and b) with one coupon of each Al alloy as a working electrode embedded in each sample. One replicate was used per type of matrix and Al alloy. As for the counter electrode, a graphite rod of 0.5 cm was embedded. The distance between the working and counter electrodes was 1 cm. An Ag/AgCl was used as a reference electrode, immersed in the external water for each measurement, as shown in Fig. 1c. The E_{corr} measurements are referred to as the Standard Hydrogen Electrode (SHE).

Table 5
MKPC and Portland-based matrix: geometry, curing conditions and test type.

		Cement paste 3 × 3 × 3 cm^3		Mortar 4 × 4 × 4 cm^3			
Binder		MKPC	CEM I	MKPC	CEM I	CEM IV	CEM I + SF
Curing condition		Isolated (in film)		1st, 2nd Water Imm		1st Water Imm	
Total test duration		1 year	4 months	550 days	550 days	300 days	300 days
Metal embedded		Pure Al (A1050)		Pure Al (A1050) & Al–Mg (AA5754)			
Type test	Corrosion rate			✓	✓	✓	✓
	Volume of H_2			✓	✓	✓	✓
	Interface (SEM/EDX)			✓	✓		
	Interface (XCT)	✓	✓				
	Porosity (MIP)			✓	✓		
	Pore solution (IC, pH)			✓	✓	✓	✓

An Autolab AUT84750 potentiostat/galvanostat was used and driven by NOVA 1.10.1.9 software. Polarisation resistance (R_p) was electrochemically determined using the linear polarisation resistance (LPR) technique by applying ± 20 mV polarisation range to the corrosion potential (E_{corr}) as suggested by Andrade and Alonso (2004) and Nygaard et al. (2009). A correction for the metal/mortar ohmic drop (IR) was executed at a frequency of 10 kHz and subtracted from the R_p measurement as described in Andrade and Alonso (2004). The correction of the ohmic drop is necessary for the accurate evaluation of the R_p of embedded metals for cementitious matrices due to the high electrical resistance of the mortar, as a consequence of the progressive advance of hydration, densification of the matrix and the progressive growth of corrosion products at the Al surface. R_p was subsequently employed to calculate the corrosion current density (i_{corr}) in μA/cm^2 using equation (2), as described in Stern and Geary (1957).

$$i_{CORR} = B/R_P/\ S \tag{2}$$

Where S is the exposure surface area of the Al alloy (9 cm^2 in the present study). A constant B of 26 mV was used as reported in previous papers (Fernández-García et al., 2024; Perona et al., 2023) and confirmed with the literature data (Caes et al., 2023). The corrosion rate is then expressed in μm/year using equation (3) according to the ASTM procedure G102-89 (ASTM-G102-89, 1999).

$$V_{CORR}\ (\mu m\ /\ year) = 3.27 \quad x \quad i_{Corr}/\rho \quad x \quad EW \tag{3}$$

Where V_{corr} is the corrosion rate in (μm/year), i_{corr} is the current density in (μA/cm^2), ρ is the aluminium density (2.7 g/cm^3), and EW is the equivalent weight for aluminium (9 g/equivalent).

2.3.2. Cement matrix characterisation

As mentioned in Table 5, the matrix characterisation was carried out by analysing the changes that occurred during the test. One analysis was performed for each technique at different exposure times, and no experimental errors could be derived.

Pore structure and ion concentrations in the pore solution were determined at specific exposure periods. For the pore structure, mercury intrusion porosimetry (MIP) was used to determine the total porosity and pore size distribution of MKPC and CEM I matrices. A mortar piece of approximately 1 cm^3 was taken to analyse the porosity. An AutoPore IV 9500 V1.09 serial 293 porosimeter was used. The sample was immersed in isopropanol for 24 h to remove the excess of water in the pores. The specimen was then dried in a desiccator under vacuum for 24 h before MIP analysis. The analysis was performed at the end of the experiment after 550 days of water immersion.

The internal pH and pore ion content (PIC) were determined according to the procedure described by Alonso et al. (2012). One piece of each of the four mortar systems was ground to a particle size of 80 μm, and a 1:1 solid/liquid suspension was prepared by dissolving 10 g in 10 ml of deionised water. After 5-min stirring, the solution was filtered, and the pH and pore ion content were determined. Two pH measurements were carried out at several curing ages using a Hanna HI1043 digital electrode with a pH stability range of 0–14. Calibration was performed with IUPAC pH standard solutions: 4, 7, 10 and 13 (±0.01). Inductively coupled plasma optical emission spectroscopy (ICP-OES) was used to determine the ionic composition (P, B, Mg, K, Na and Ca) using a Varian 725 ES ICP optical emission spectrometer.

2.3.3. Al/matrix interface characterisation

To study the physicochemical changes at the interface of Al alloy with the mortar matrix, a HITACHI S-4800 SEM-EDX equipment was

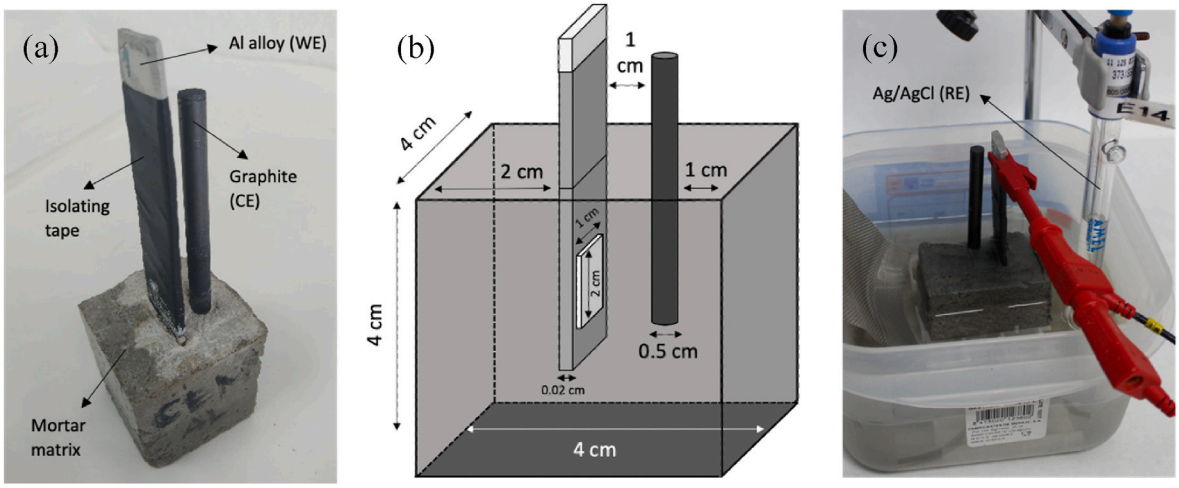

Fig. 1. Arrangements for Al corrosion characterisation: a) Mortar sample with embedded Al alloy coupon (working electrode, WE) and graphite rod (counter electrode, CE), b) cell configuration, and c) connection system with an Ag/AgCl electrode immersed in the external water (reference electrode, RE).

used in backscattering mode (SEM-BS). After 550 days of water immersion (see Table 5), MKPC and CEM I mortar matrices with pure Al (A1050) and Al–Mg alloy (AA5754) were cut to obtain a transverse section, as shown in Fig. 2 left. A piece of 2 cm^2 for each cementitious system containing the Al and mortar matrix was considered for SEM-BS interface characterisation. A BRUKER X-flash detector model 5030 was employed for EDX microanalysis. The semi-quantitative elemental exploration was driven using the software ESPRIT v.1.9. Several analyses were performed using the EDX technique at different matrix depths to account for data variability.

XCT was used to observe the physical changes that occurred at the metal/cement paste interface region using a Nikon CT-SCAN-XT H-160. The resolution of the XCT equipment varies from 3 to 79 μm, depending on the sample size. According to the present samples studied and cubic voxel size used, the resolution achieved 25.6 μ m^3. As shown in Table 5, this test was performed at the end of the experiment in MKPC and CEM I pastes with pure Al embedded. One sample for each type of cement was used. Fig. 2 right also shows the cement configuration for XCT analysis. A total of 1600 images were taken for each analysis performed. The data was processed using DragonFly® 2022 software, which allowed the generation of 2D and 3D images as well as the determination of the porosity percentages.

3. Results

3.1. Aging of pore water pH and ion content of cementitious matrices in water immersion

The pH of the pore solution is an essential factor in cementitious systems that determines the range of passivity of Al and the associated corrosion phenomena (Pourbaix and Burbank, 1964; Vargel, 2020). To understand the consequences on the Al corrosion performance, the pH and the evolution of the ion concentration of the pore solution were determined for MKPC, CEM I, CEM IV, and CEM I+50%SF mortars immersed in water following the procedure described in the experimental part. Furthermore, the ions released into the external curing water were analysed, as shown in Table 6.

For MKPC matrices, a decrease in the pore main ions content (P, Mg, K, Na and B) is observed over time. A similar effect was found in Fernández-García et al. (2024) in 100% RH associated with the progression of the acid-base reaction (KH_2PO_4 and MgO). In the present study, using water immersion, another important process has also been considered, which is related to the release of the pore ions to the external solution, indicating that leaching from the matrix occurred, as suggested by Chong et al. (2017). Diaz Caselles et al. (2024a) noted that K-struvite from MKPC pastes has a high solubility in water. The presence of Na in the pore solution and in the external water is derived from the FA used as filler. The procedure used to determine the pore ion composition may result in a partial dissolution of the K-struvite. This method, described by Alonso et al. (2012) for Portland cement, is not calibrated for MKPC

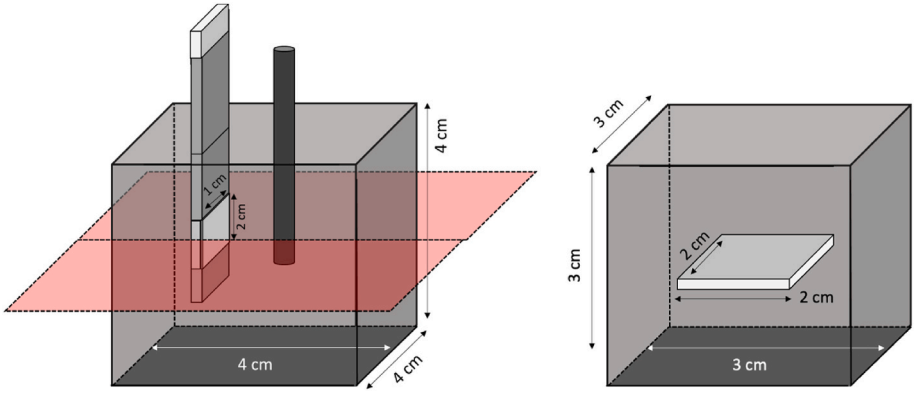

Fig. 2. System configuration for SEM-BS/EDX (left) and XCT (right) techniques for metal/matrix interface studies.

Table 6
Pore ion content of the pore solution and the external curing water of the different MKPC, CEM I and Portland cement blended mortars using ICP-OES (in mmol/L).

Binder	Water	Time	P	B	Mg	K	Ca	Na
		(days)	(mmol/L)					
MKPC	Pore	7	212.21	18.41	2.47	719.06	–	3.35
		300	7.31	1.67	0.63	21.52	–	2.99
		250[a]	6.55	1.62	0.42	15.66	–	0.56
	External	300	6.71	1.66	0.37	15.56	–	0.46
		250[a]	3.88	0.91	0.02	11.38	–	0.37
CEM I	Pore	300	–	–	–	4.22	13.68	1.73
		250[a]	–	–	–	1.96	8.56	0.66
	External	300	–	–	–	2.56	0.72	0.24
		250[a]	–	–	–	1.14	0.64	0.14
CEM IV	Pore	300	–	–	–	3.07	7.71	1.83
	External	300	–	–	–	0.95	1.43	0.26
CEM I+50%SF	Pore	300	–	–	–	2.06	2.20	1.73
	External	300	–	–	–	0.46	1.29	0.17

[a] Second period duration in renewed external deionised water.

systems. However, it does allow for the monitoring of the matrix's evolution. The ion diffusion to the external curing water is attenuated in the renewed water in the second testing period, for a similar exposure age (250 days). The amount of ion leached is less relevant in the case of CEM I, CEM IV and CEM I+50%SF, probably due to less ion content in the pores and lower solubility of the solid phases mainly associated with Ca, K and Na.

Changes in the ion content of the pore solution can affect the internal pH. Fig. 3 shows the evolution of the pH of the internal pore solution over time in all cementitious matrices.

In CEM I, CEM IV and CEM I+50%SF matrices (see Fig. 3 left), initial high alkaline pH values (12.7 ± 0.1 for CEM I and CEM IV) are measured due to the presence of portlandite and alkalis in the pore solution, with a constant evolution throughout the test (12.6 ± 0.1), as also observed by Cau Dit Coumes et al. (2014), Kinoshita et al. (2013), and Perona et al. (2023) with pH values ranging from 12.5 to 13 in CEM I systems under isolated and immersed in water conditions. In contrast, CEM I+50%SF with an initial high alkaline pH of 12.6 ± 0.1 shows a significant decrease up to 70 days due to the depletion of portlandite by the pozzolanic reaction with SF (pH 10.5 ± 0.1), which remains around this pH values until the end of the test (300 days in water immersion). This positive evolution of the pore solution pH due to the addition of SF against the highly alkaline CEM I matrix was also noted by García Calvo et al. (2010) under 98% RH condition.

Fig. 3 right shows a constant evolution of the pore solution pH in MKPC mortar matrix up to 50 days immersed in water (pH 7.7 ± 0.1), as also observed by Cau Dit Coumes et al. (2014), Fernández-García et al. (2024), and Perona et al. (2023) under different curing conditions (isolated and immersed in water). A significant increase in the internal pH is observed after 300 days of water immersion (from 7 ± 0.1 to 9.8 ± 0.1). This increase in the pore solution pH is attributed to the reduction of phosphates in the pore solution due to a leaching process to the external curing water, as observed in Table 6, and the progressive advance of the acid-base reaction. After 250 additional days of immersion in renewed deionised water, the internal pH remained constant at around 9.7 ± 0.1 with a less intense leaching process of the phosphate content of the pore solution to the external curing water. This effect of the ion diffusion and leaching process in the pore solution pH may be influenced by the pore size and pore structure of the matrix, as described later.

3.2. Pore structure characteristics of mortar matrices

To understand the effect of water media in matrix alteration, the pore network of CEM I and MKPC matrices was evaluated at the end of the tests by analysing the total porosity and pore volume distribution. In water immersion, the MIP analyses provided a lower total porosity of 8.1% in CEM I mortar, compared with 12.3% for MKPC mortar. The main difference in total porosity between CEM I and MKPC is related to the differences in pore size distribution, as observed in Fig. 4. The pore volume as a function of the pore diameter is shown in Fig. 4 left. It is observed that the CEM I matrix shows a unimodal distribution with a clearly defined zone of cumulative capillary pores in the region between 0.1 and 0.01 μm (see Fig. 4 right), which reduces the total porosity.

A multimodal pore volume distribution is identified in Fig. 4 left for the MKPC matrix with no dominant pore region. The pore sizes in the matrix are distributed in a larger pore region (between 10 and 0.1 μm), contributing to an increase in the total porosity, as depicted in Fig. 4

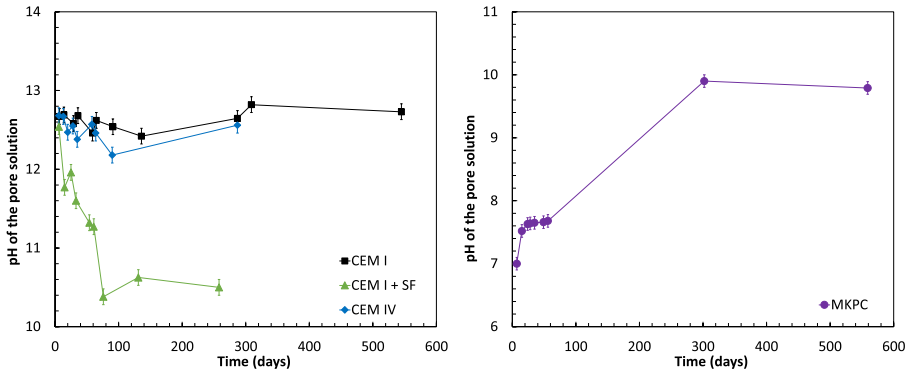

Fig. 3. Evolution of the pH of the internal pore solution of CEM I and blended Portland cement (CEM IV and CEM I+50%SF) (left) and MKPC (right) mortar matrices.

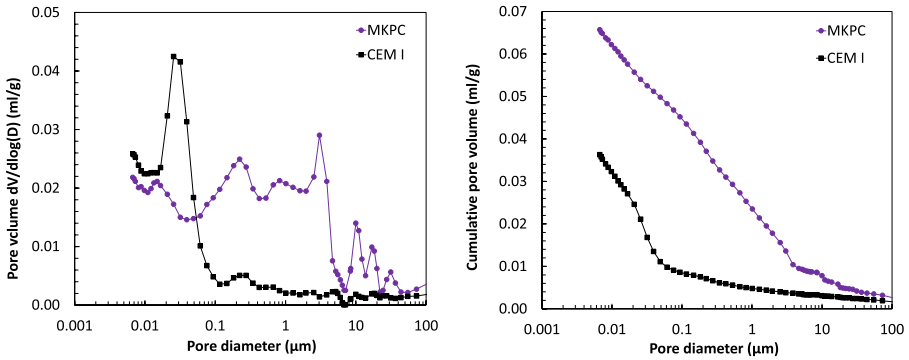

Fig. 4. Pore volume (left) and cumulative pore volume (right) distribution in MKPC and CEM I mortar systems.

right. This finding is in agreement with Chong et al. (2017), who attributed this phenomenon to a lower formation of reaction products in water immersion conditions. However, as defined by Fernández-García et al. (2024), higher moisture content in the pores without leaching also increases the total porosity in 1M MKPC mortar samples. Despite this, the pore structure and pore size distribution in the MKPC matrix can favour the leaching process and ion diffusion during the interaction with the curing water.

3.3. Corrosion reactivity of pure Al (A1050) and Al-3.5%Mg alloy (AA5754)

To understand the Al reactivity in contact with different cement composites, the interaction of pure Al and Al–Mg alloy with MKPC, CEM I, and blended Portland cement matrices (CEM IV and CEM I+50%SF) was studied in water immersion.

To identify the main differences between the types of cement, Fig. 5 shows the relationship between corrosion potential (E_{corr}) and current density (i_{corr}) calculated using equation (2). The Al alloys in the MKPC matrix showed more anodic E_{corr} and lower i_{corr} values at the initial stage of the interaction than the alkaline CEM I and Portland blended matrices, probably due to its initial near-neutral pore solution pH for Al passivation (see Fig. 3 right). The i_{corr} in the MKPC matrix decreased more than two orders of magnitude (from 0.5 to 0.001 μA/cm^2) as E_{corr} decreased over time (from −1.2 to −0.2 V), somewhat higher at the early ages for the Al–Mg alloy due to the Mg reactivity contribution. Fernández-García et al. (2024) pointed out that the almost neutral pH of the MKPC matrix is expected to be detrimental to the passivation of Mg metal (passivation pH of Mg ranges between 11 and 14, according to Pourbaix and Burbank (1964)), increasing the corrosion reactivity for the Al–Mg alloy. Less i_{corr} (from 10 to 0.001 μA/cm^2) was identified with time for the CEM I+50%SF matrix, associated with a decrease in the internal pH (Fig. 3 left). The highest corrosion levels ($E_{corr} \approx 1.6$ to 1.4 V, $i_{corr} \approx 100$ to 0.10 μA/cm^2) were detected for CEM I and IV matrices without significant differences between both alloys.

To understand the i_{corr} evolution, Fig. 6 shows the corrosion rate (V_{corr}) versus time in μm/year based on equation (3). In water immersion, the corrosion rate in all cementitious matrices tends to decrease with ageing. MKPC mortar showed the lowest corrosion rate values (5–0.012 μm/year), as Delpech et al. (2017) also noted. CEM I+50%SF mortar showed higher initial corrosion rates (from 150 to 0.02 μm/year for Al and 150 to 0.08 μm/year for Al–Mg) approaching MKPC after 300 days of testing. Compared to the MKPC matrix, two orders of magnitude higher values were detected in the highly alkaline CEM I matrix, followed by the CEM IV matrix (170–0.4 μm/year), similar to that found by Caes et al. (2023), and Delpech et al. (2017) under immersion and isolated condition, respectively. A similar trend in the corrosion rate evolution was found for Al and Al–Mg, although slightly higher V_{corr} values were detected for the Al–Mg alloy due to the greater corrosion reactivity

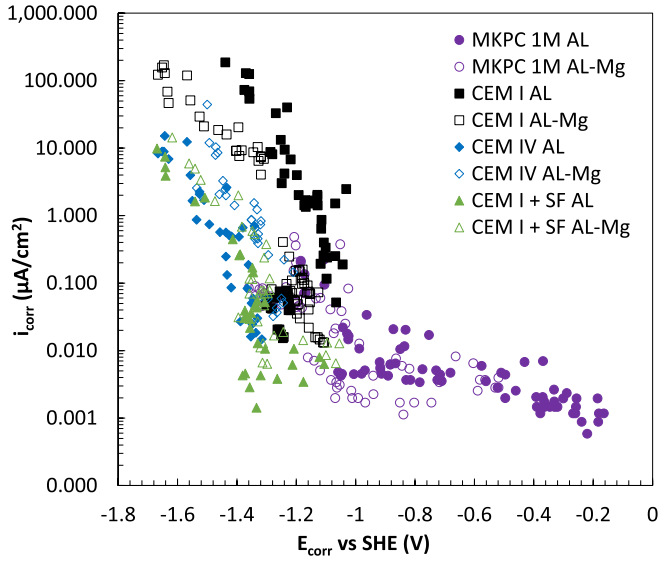

Fig. 5. E_{corr} (vs SHE) versus i_{corr} in MKPC and Portland-based matrices over 550 days.

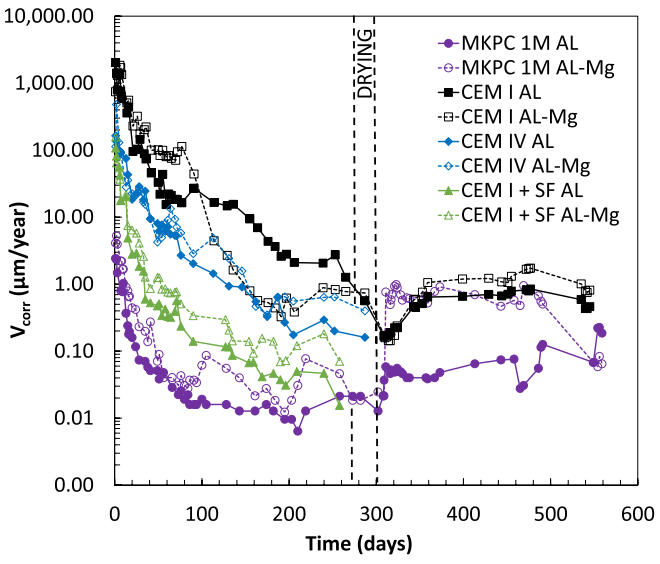

Fig. 6. Corrosion rate (V_{corr}) over time for pure Al and Al–Mg alloy in MKPC, CEM I and Portland cement blended matrices.

considered from the E_{corr} of the Mg alloy.

After 300 days of water immersion, only MKPC and CEM I mortars were dried and the immersion was extended for another 250 days in renewed water. Fig. 6 shows a reactivation in both matrices due to the return to the water media. The increase in the moisture content in the pores at the Al surface after the drying period contributed to a significant increase in the corrosion rate, as Fernández-García et al. (2024) suggested. This effect is more pronounced in the Al–Mg alloy in the MKPC matrix (with a pH from 7 to 9.8, see Fig. 3 right) which still remains outside the optimal range of pH for Mg passivation (11–14) (Pourbaix and Burbank, 1964). In addition, the contribution of Mg to the Al corrosion increased with the higher content of Mg in the metal alloy, as observed by Poras et al. (2023). After 550 days of testing, Al–Mg alloy reached the same level as pure Al (0.05 μm/year), due to the increase of MKPC internal pH to nearly 10. After the drying period, the CEM I matrix evolved to higher corrosion rates, which remained constant at the end of the test (0.81 μm/year). The high pore solution pH (see Fig. 3 left) and pore water saturation can favour the corrosion process in the CEM I matrix.

3.4. Physico-chemical changes at the Al/matrix interface

To observe the Al reactivity in different cementitious systems, SEM-BS coupled with EDX analyses were carried out to study the physico-chemical alterations at the metal/matrix interface after 550 days of water immersion. Fig. 7 shows the Al-3.5%Mg metal surface in contact with a CEM I (Fig. 7 left) or an MKPC (Fig. 7 left) matrix using 50× magnification images. Large differences were detected at the metal/matrix interface depending on the cement composition, which are analysed separately: 1) at the metal surface and 2) at the matrix level.

3.4.1. Changes on the Al metal surface

Fig. 8 left shows the zoomed surface of the Al alloy after 550 days of interaction with the CEM I matrix, marked in Fig. 7 left in a yellow area. The high alkalinity of this type of matrix leads to corrosion of the Al metal. A corrosion product is formed with a heterogeneous distribution along the Al surface, with a thickness from 50 to 90 μm. The EDX spectra of the corrosion product are included in Fig. 9 left at different depths from the Al surface (10, 50 and 90 μm), numbered in Fig. 8 left as 1, 2 and 3. The composition of this product mainly consists of aluminium and oxygen, with some residual magnesium content, as also noticed by Caes et al. (2023), and Mendibide et al. (2021).

Fig. 8 right displays the zoomed area of the MKPC matrix interface in contact with Al alloy, marked in Fig. 7 right in a yellow area. No visible corrosion product layer was detected. It appears that the lower Al reactivity is most likely due to the lower internal pH of the MKPC matrix (from 7 to around 10). However, a region of the MKPC matrix with an apparently high density compared with the rest of the matrix was observed in the SEM-BS image (see Fig. 8 right), referred to as a "layer" due to its homogeneous distribution along the Al surface, with a thickness of about 30 μm. The EDX spectra of this MKPC interface region are displayed in Fig. 9 right from the local analyses at different depths from the Al surface (10, 30 and 70 μm) numbered in Fig. 8 right as 1, 2 and 3. The composition of this "layer" is constituted of the characteristic components of an MKPC matrix: P, Mg and K.

3.4.2. Changes in the mortar matrix

The compositional maps presented in Fig. 10 allow the identification of the alteration of the CEM I and MKPC matrices due to the Al interaction. A zoomed image from Fig. 7 was considered, removing the Al metal for the SEM-EDX analyses due to the high metal reflectivity, which can affect the characterisation. The upper part of the images corresponds to the nearest zone in contact with the Al metal. Table 7 summarises the average elemental composition and deviations obtained from EDX microanalyses in various zones of the matrix at different distances from the interface, shown in Fig. 10.

An Al enrichment is detected in the CEM I matrix (see Fig. 10a). EDX analyses in Table 7 confirm that the aluminium content in the CEM I matrix decreases from 26.1 ± 5.5% near the Al surface (≈0.8 mm, zone 1) to 1.5 ± 0.3% far from the Al surface (≈7.5 mm, zone 3). To that depth, the Al reacts with other CEM I matrix components, such as Ca and sulfate ions, forming ettringite as the main reaction product. EDX analyses (see Table 7) confirmed the formation of the ettringite nodules: 39.7 ± 3.1% Ca, 12.1 ± 0.3% S and 7.4 ± 1.8% Al [$(CaO)_6$-(Al_2O_3)–$(SO_3)_3$–$32H_2O$]. Fig. 10b shows an ettringite nodule with a well-defined morphology. Microcracks in the paste near ettringite are observed, probably due to the deformations induced by its higher volume, affecting the surroundings of the waste-form stability, as previously suggested by Diamond (1996).

The Al reactivity in an MKPC matrix is shown in Fig. 10c, thanks to the compositional map spectra. EDX average data and deviations presented in Table 7 indicate that the zones analysed (Z6, Z7, Z8), shown in Fig. 10c, have a similar composition, constituted by 17.9 ± 1.4%P, 13.0 ± 1.7% Mg, and 19.9 ± 1.5% K. The Ca, Si and Al contents are attributed to the FA used as a filler in the MKPC formulation, which is homogenously distributed in the matrix. The Al reaction product is not detected, as in the case of CEM I, although the pH of the pore solution is increased from near neutral to around 10 (see Fig. 3 right). The acid-base reaction of the main components in the MKPC matrix microstructure corresponds to the formation of K-struvite: 19.5 ± 0.6% P, 14.3 ± 3.8% Mg, and 24.4 ± 5.0% K [$KMg(PO_4)\cdot 6(H_2O)$]. Fig. 10d shows a typical columnar K-struvite morphology related to a well-defined crystal formation.

3.5. Physical changes at the Al/matrix interface

In cementitious matrices, the presence of pores has a complex effect on the physical stability. Fig. 11 shows a series of 2D images corresponding to the CEM I and MKPC pastes at an initial time of 7 days and after 4 months (CEM I) and 1 year (MKPC) of ageing under isolated conditions in plastic films (endogenous curing without external moisture

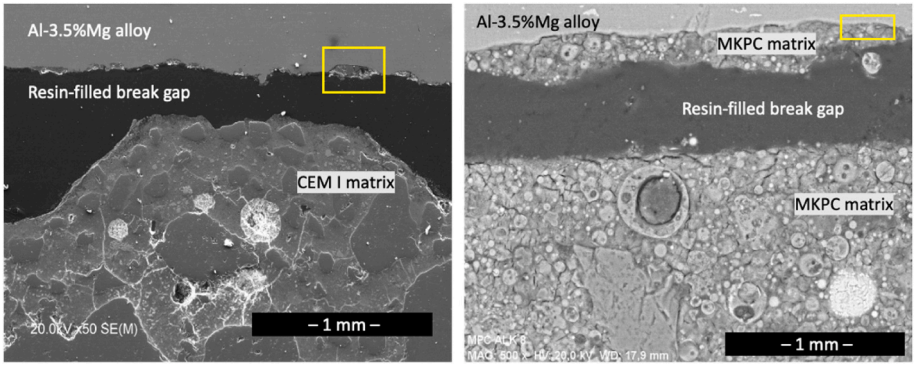

Fig. 7. SEM-BS images of Al–Mg interface with CEM I (left) and MKPC (right) matrices.

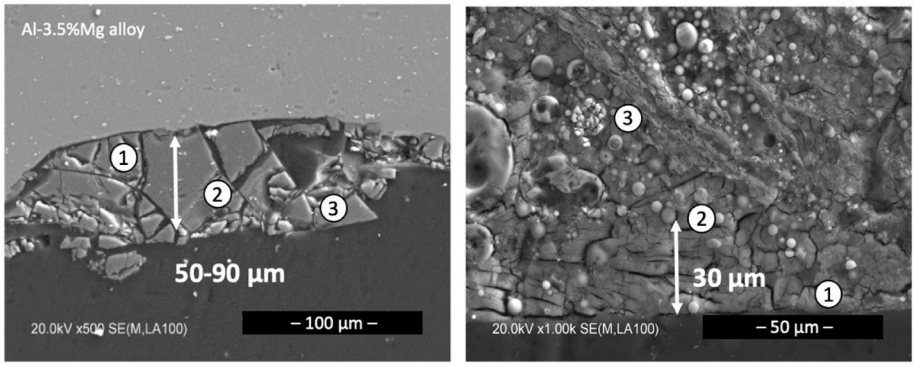

Fig. 8. Zoomed areas at the interface between Al–Mg with CEM I (left) and MKPC (right) matrices, marked in Fig. 7. (The numbers indicate the EDX local analyses in Fig. 9).

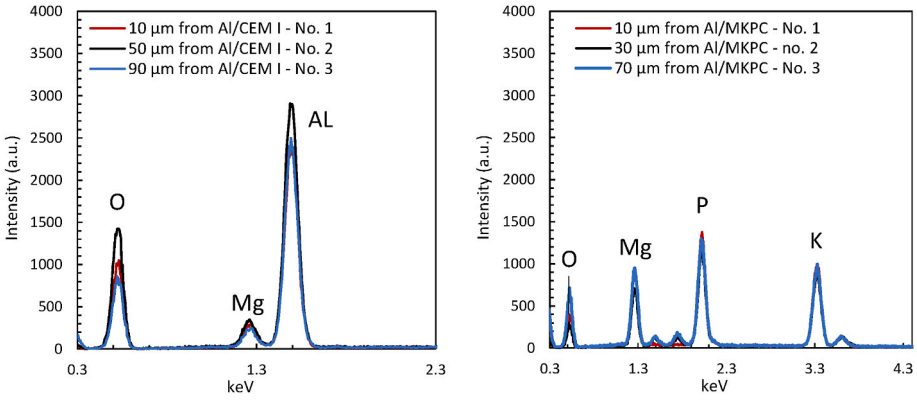

Fig. 9. EDX spectra from microanalysis of Al alloy interface with CEM I (left) and MKPC (right) matrices at different depths from the metal surface.

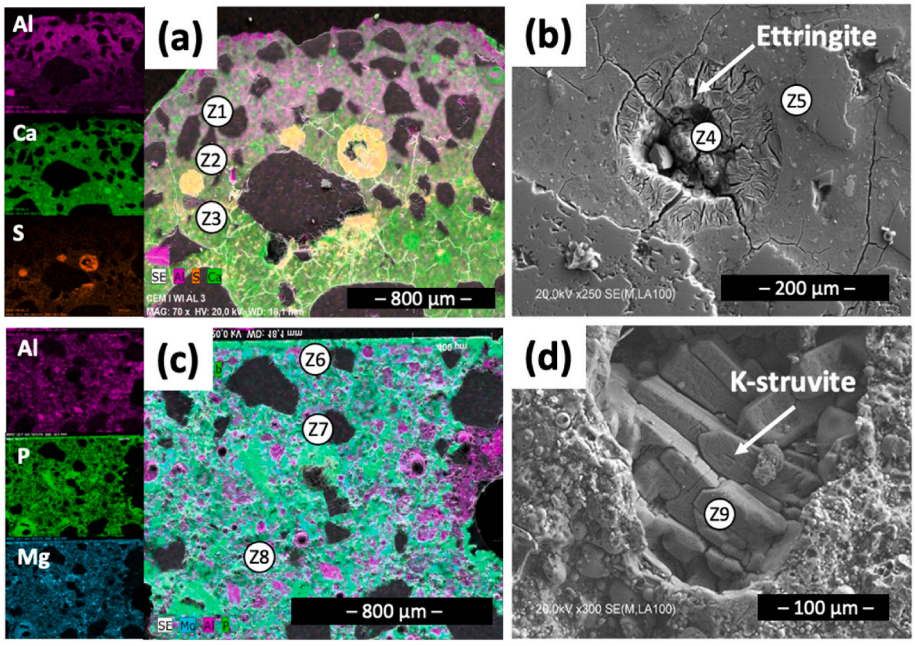

Fig. 10. SEM-BS images of a) chemical composition maps of metal/CEM I matrix interface (zones: Z1, Z2, Z3), b) ettringite zone (zones: Z4, Z5), c) chemical composition maps of metal/MKPC matrix interface, (zones: Z6, Z7, Z8) and d) K-struvite morphology (zone: Z9).

supply). The microtomography study generated around 1600 images per sample, which do not always coincide with the exact layout of the aluminium plate. It can be observed that there is a high porosity around the aluminium plate in the CEM I pastes highlighted in blue in Figs. 11a and b after 7 days and 4 months of interaction, which is attributed to the larger volumes of H_2 released due to the higher Al reactivity in this alkaline matrix. However, no associated swelling and cracking was detected in the monolith. This porous transition zone in the Al/CEM I

Table 7
EDX elemental microanalysis zones of CEM I and MKPC matrices due to Al reactivity (in wt. %).

	EDX analysis	Matrix Depth	P	Mg	K	Al	Si	Ca	S
		(mm)	(% weight)						
CEM I	Zone 1 (Z1)	0.8	–	–	–	26.1±5.5	8.9±2.1	19.6±5.2	0.0±0.0
	Zone 2 (Z2)	1	–	–	–	6.7±2.8	5.3±2.9	45.0±6.6	0.0±0.0
	Zone 3 (Z3)	7.5	–	–	–	1.5±0.3	11.7±0.9	48.1±1.1	1.6±0.1
	Zone 4 (Z4)	1	–	–	–	7.4±1.8	0.0±0.0	39.7±3.1	12.1±0.3
	Zone 5 (Z5)	1	–	–	–	6.8±2.4	8.3±2.9	46.7±1.6	1.3±0.1
MKPC	Zone 6 (Z6)	0.2	19.4±0.5	14.2±1.4	21.6±1.9	0.7±0.5	0.4±0.3	2.4±1.6	–
	Zone 7 (Z7)	0.6	17.7±1.2	13.8±1.3	19.5±2.2	1.8±0.4	2.5±1.1	2.5±2.7	–
	Zone 8 (Z8)	1	16.7±1.7	11.1±1.9	18.8±3.3	2.2±2.5	5.46±2.33	2.4±2.8	–
	Zone 9 (Z9)	0.6	19.5±0.6	14.3±3.8	24.4±5.0	0.1±0.2	0.1±0.1	1.2±0.1	–

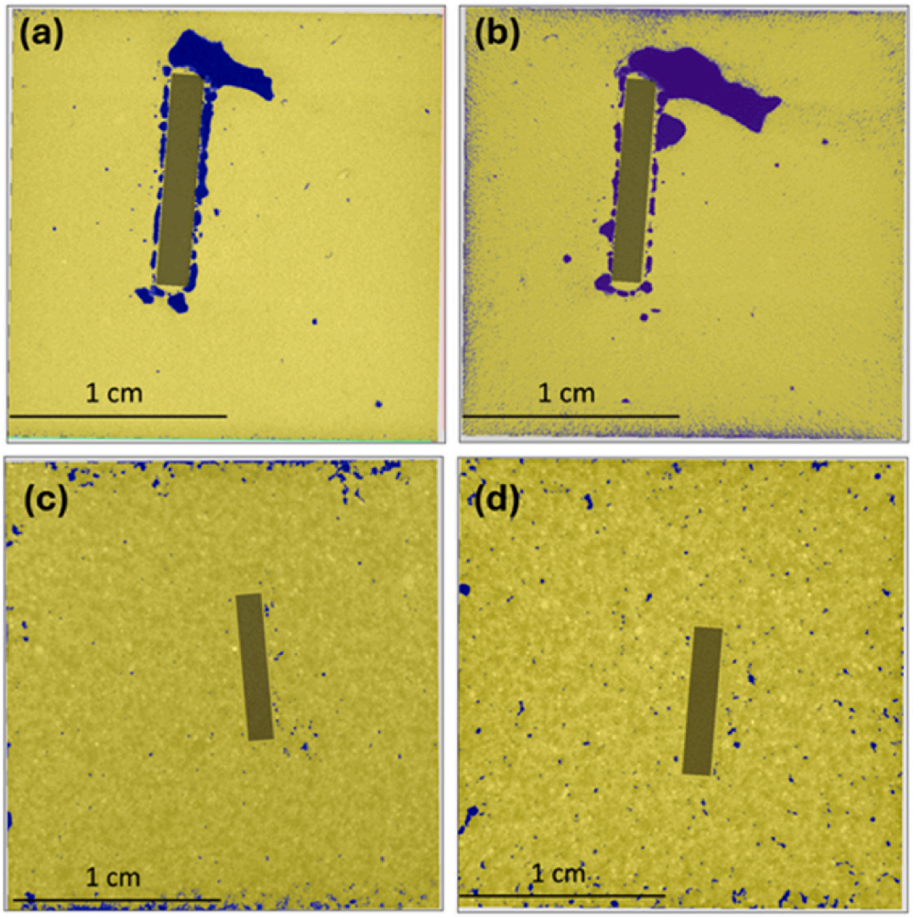

Fig. 11. 2D XCT images: a) CEM I paste t = 7 days, b) CEM I paste t = 4 months, c) MKPC paste t = 7 days and d) MKPC paste t = 1 year. Legend: blue colour = porosity; yellow colour = matrix; brown colour = Al plate.

matrix interface was previously observed by Setiadi et al. (2006) using the SEM/EDX technique.

The pore region around the Al increased with the ageing of the CEM I system. Also, a less dense region with higher porosity was observed in the external part of the monolith, as well detected in Fig. 12b. In the case of the MKPC matrix (Fig. 11c and d), less porosity was observed in the cement paste at the interface of the Al/matrix, indicating the lower reactivity between both materials, but higher pore regions distributed in the paste were also detected, probably due to the pore water consumption for the acid-base reaction progress in an MKPC matrix under isolated conditions, resulting in more air-filled pores, as also noted by Fernández-García et al. (2024).

The 3D images (Fig. 12) show half of the monoliths with the total porosity distribution on the visible faces, and the whole monolith's contours are shown in grey. The CEM I porosity observed in 3D is homogeneously distributed in the matrix (see Fig. 12a), which increases in the surface of the sample after 4 months (≈1 mm thickness) (see Fig. 12b). In contrast, the MKPC paste shows a high porosity in the outer contour of the sample after 1 year by the direct contact of the monolith with the curing media (≈1 mm thickness) with a more heterogeneous distribution in the matrix (Fig. 12c and d).

A quantitative analysis was carried out on the volume fractions of components of both matrices at the initial and long-term curing ages. The procedure allows quantifying the porosity for each matrix (see Fig. 13). Porosity was increased with ageing in both systems. The CEM I matrix reached a higher porosity, increasing by 8% in 4 months. The MKPC matrix only increased its porosity by nearly 1% after 1 year with <0.7% sample expansion. These results align with the MIP

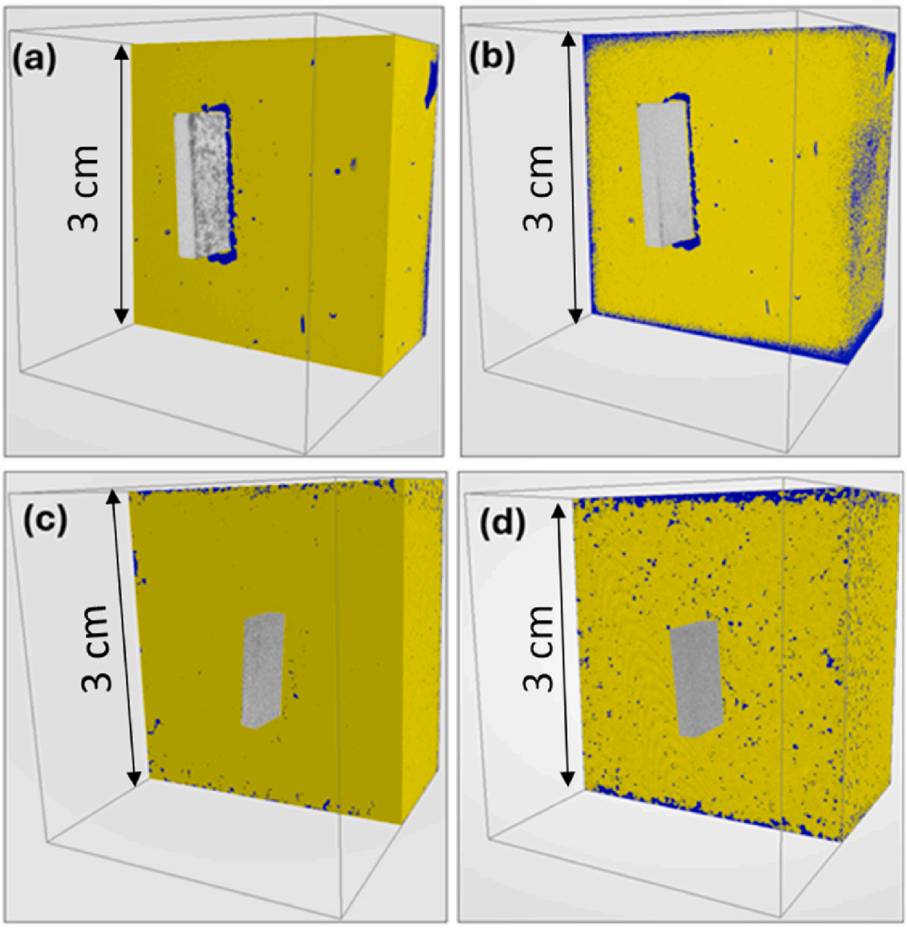

Fig. 12. 3D XCT images: a) CEM I paste t = 7 days, b) CEM I paste t = 4 months, c) MKPC paste t = 7 days and d) MKPC paste t = 1 year. Legend: blue colour = porosity; yellow colour = matrix; grey colour = Al plate.

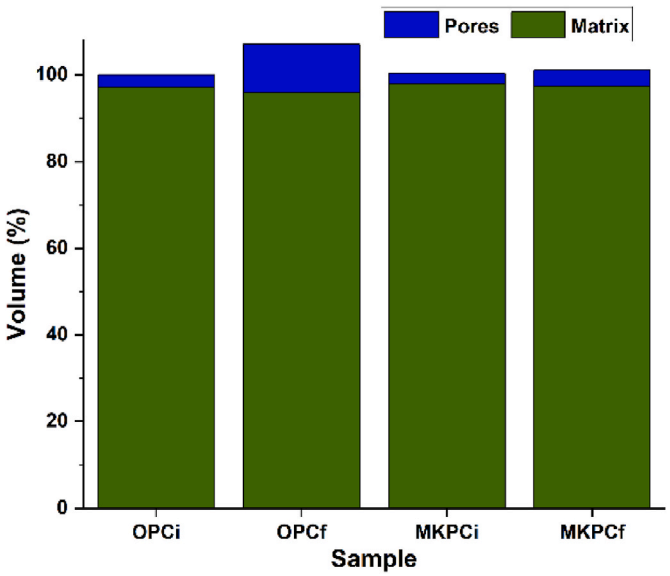

Fig. 13. Pore volume in CEM I and MKPC pastes with hydration time. Legend: I = start time; f = end time. Values exceeding 100% indicate expansion.

measurements.

Despite all samples being wrapped in plastic films within a chamber set at a constant temperature, the XCT analyses indicated that the prominent increase in porosity occurred on the outer contours of the MKPC monolith, as these surfaces were more exposed to interaction with the curing media. Therefore, an additional analysis was performed by discarding the outer 5 mm of each cubic surface to identify the porosity's internal evolution. Fig. 14 compares the effect of this additional treatment and confirms that the porosity in MKPC paste increased mainly in the outer contour (Fig. 15). It is well known that MKPC reacts rapidly to form K-struvite, but Padilla-Encinas et al. (2024) observed for similar formulations that the mechanical strength attributed to K-struvite formation may not have reached a plateau even after 90 days of reaction, indicating that the incorporation of water from the pore water to form K-struvite is a rapid initial process that evolves slowly with curing time. Under these circumstances, water from the outer surfaces of the MKPC paste may end up being lost more rapidly by interaction with atmospheric gases than being incorporated into the K-struvite structure.

4. Discussion

4.1. Consequences of reactivity in the Al/matrix interface

Simultaneous analyses of the metal corrosion response and the physicochemical changes at the metal/matrix interface and pore characteristics were evaluated to increase the understudying of Al reactivity in contact with different cementitious matrices and the consequences of this process.

The pore characteristics of the MKPC, OPC type CEM I and Portland blended systems influence the Al corrosion reactivity. Fig. 16 illustrates the relationship between the corrosion rate (μm/year) and the pore

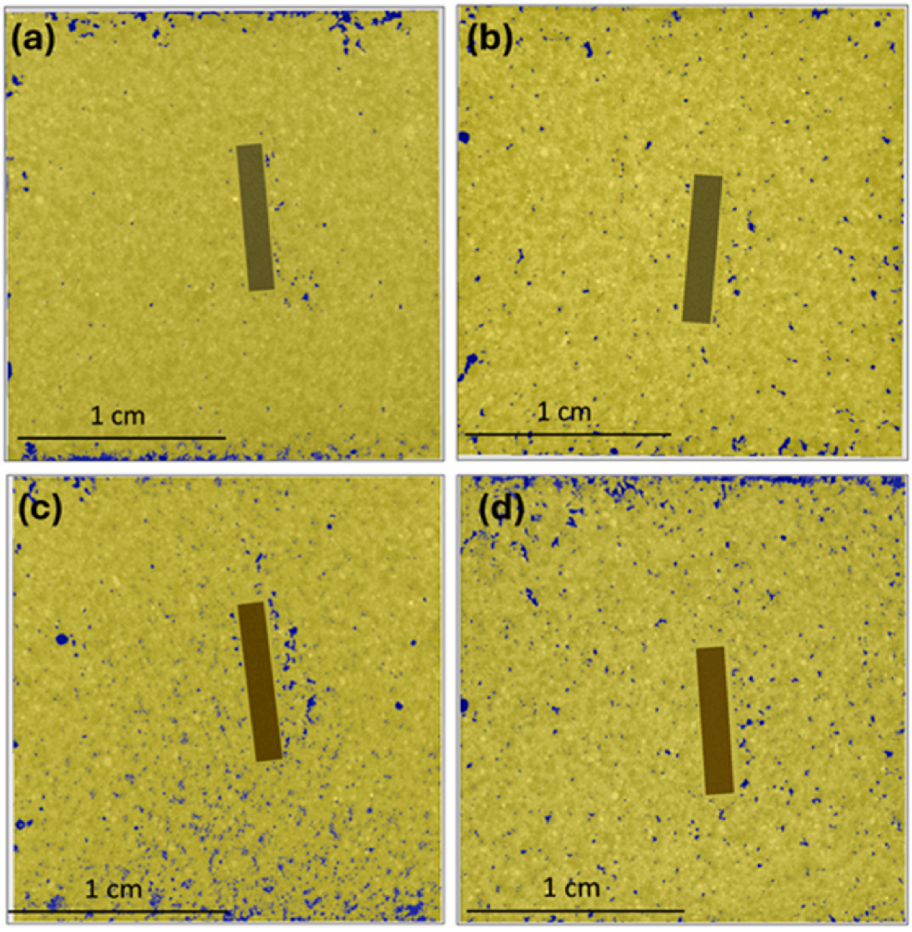

Fig. 14. 2D XCT images: a) MKPC paste t = 7 days, b) MKPC paste t = 1 year, c) MKPC paste section t = 7 days and d) MKPC paste section t = 1 year. Legend: blue colour = porosity; yellow colour = matrix; brown colour = Al plate.

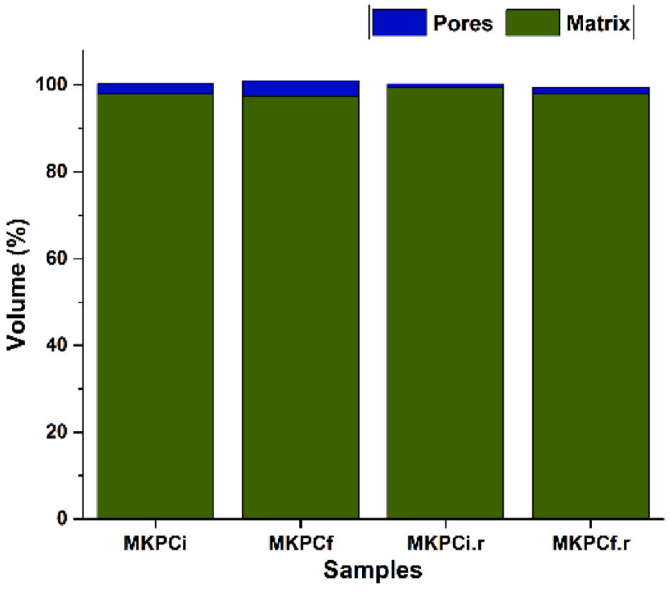

Fig. 15. Pore volume in MKPC and trimmed MKPC pastes with reaction time. Legend: i = start time; f = end time.

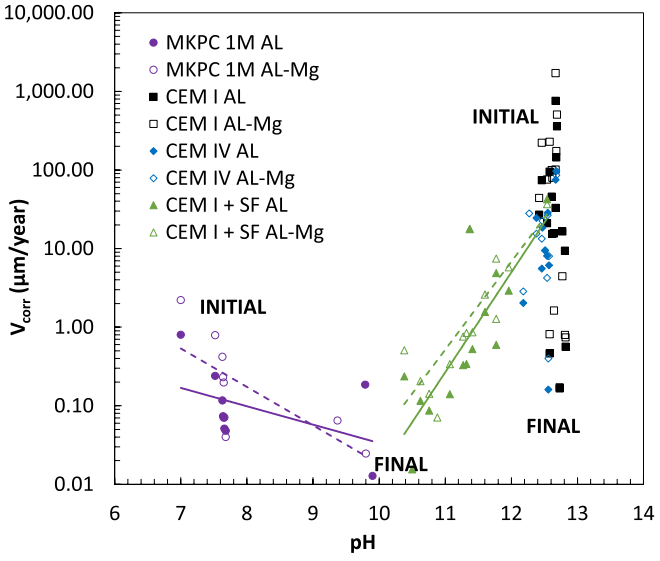

Fig. 16. Corrosion rate (V_{corr}) as a function of the pore solution pH in MKPC, CEM I, CEM IV and CEM I+50%SF matrices.

solution pH of the cementitious materials. The highly alkaline matrices (CEM I and IV) with high internal pH show higher corrosion rates over time. Conversely, the MKPC matrix followed by CEM I+50%SF shows the lowest corrosion rates due to their lower pore solution pH, which is more suitable for the passivation of radioactive Al. In the case of the MKPC matrix, an evolution to higher internal pH has not significantly

affected the corrosion rate, following the decreasing trend over time, as shown in Fig. 6. However, a significant drop in the pore solution pH of the CEM I+50%SF matrix shows a clear evolution towards lower corrosion rates with ageing, approaching that of the MKPC system.

Furthermore, the ion concentration of the pore solution and pore network structure also influence the electrochemistry of Al. Higher porosity with a pore network dominated by intermediate pores allows ion diffusion to the external curing water, changing the ionic concentrations in the pore solution over time, as Chong et al. (2017) suggested. As a result, there is an increase in the pH up to 9.8 in the pore solution of MKPC matrices, associated with a leaching phenomenon of phosphate ions and a decrease at the interface with the Al alloy, causing the increase in pH. In addition, borate ions increase the pore solution pH of the MKPC matrix through the leaching phenomenon, as suggested by Diaz Caselles et al. (2024b). However, the phosphate content in the MKPC system plays a vital role in the Al/matrix interaction, lowering the internal pH and forming a protective film on the metal surface (Fernández-García et al., 2024; Wang et al., 2022).

In the present study, a P/Mg/K dense "layer" was found at the Al/MKPC matrix interface, which did not show a relevant increase in reactivity even with an increase in pH, probably because the passive layer formed can resist this increase in pH. The pH of the pore solution remains constant in a CEM I matrix due to the presence of portlandite, which buffers the pH of the pore solution. The higher Al reactivity in the CEM I system is confirmed by the formation of a thick layer of corrosion products of aluminium and oxygen at the metal/matrix interface. In addition, this high reactivity generates an excess of Al ions released into the cement matrix, as observed by Caes et al. (2023), and Mendibide et al. (2021). The Al ions from the Al metal corrosion that penetrate the matrix can lead to the formation of expansive ettringite, confirming that OPC type CEM I are not appropriate for Al immobilisation. In addition, a region with high porosity in the Al/matrix transition zone was observed by XCT in a CEM I paste compared to MKPC, as suggested by Setiadi et al. (2006). This gap increased with exposure time is attributed to the release of H_2 bubbles resulting from the high reactivity of Al in this high alkaline matrix (CEM I). A volume increase of 7% was detected in the CEM I monolith. These volume expansions in CEM I at the Al/matrix interface and the H_2 release associated with Al reactivity could lead to loss of stability of the waste-form. In contrast, the MKPC matrix only increased its porosity by nearly 1% after 1 year at the interface, and the total sample expansion is negligible (<0.7%) due to a lower Al reactivity.

4.2. Quantification of H_2 released associated with the Al reactivity

As mentioned above, the quantification of the volume of H_2 released due to the contact between the Al alloy and the cement matrix is necessary to identify an optimal cementitious material for Al immobilisation. Corrosion rates obtained using the R_p values from LPR measurements allow to quantify the volume of H_2 release from pure Al and Al–Mg alloy in each type of cementitious matrix. Calculation based on the Faraday's law was performed using the following equations (4) and (5), proposed elsewhere (Fernández-García et al., 2024; Perona et al., 2023; Delpech et al., 2017),

$$W_{Loss}(Al) = (Q_{acum}\ x\ Mass\ (Al)) / (n\ x\ F) \quad (4)$$

$$V\ (L) = [(3 / 2)\ x\ (W_{Loss}\ (Al) / Mass\ (Al))\ x\ ((R\ x\ \ T) / P)]\ /\ S \quad (5)$$

where W_{Loss} is the weight loss of Al (g), Q_{acum} is the accumulated charge (C), Mass (Al) is the molecular weight of Al (26.98 g/mol), n is the number of moles of aluminium in the reaction, F is the Faraday's constant (96485 C/mol), R is the gas constant (0.082 atm L/K mol), T is the absolute temperature (298 K), P is the pressure (1 atm), and S is the Al surface (9 cm^2).

Fig. 17 left shows the main differences in the H_2 gas production for the four cementitious materials over 300 days in water immersion. As the first measurement was taken 24 h after mixing (see Methodology Section), the statistical function was adjusted to estimate the H_2 produced during the first 48 h of interaction. This estimation is displayed in Fig. 17 right. It can be seen that the first 48 h of interaction are crucial in the production of H_2 gas. However, the highest amount of H_2 release was observed in the CEM IV matrix for Al–Mg alloy of about 4 L/m^2, representing 13% of the total volume release over 300 days of water immersion (≈30 L/m^2, see Fig. 18 left).

The accumulated H_2 gas in Fig. 17 left for 300 days in water immersion shows that the highest H_2 production was detected in the CEM I and IV matrices related to their high alkaline pore solution pH (see Fig. 3). Accumulated H_2 values of nearly 20 and 30 L/m^2 for Al and Al–Mg were detected in CEM I and IV systems, as observed in Fig. 18 left. However, more than one order of magnitude lower H_2 volume was detected in the CEM I+50%SF matrix (≈8 L/m^2) due to decreased pore solution pH to a less aggressive value (pH = 10.5). Similar pH values of this low pH matrix were found by García Calvo et al. (2010) at 90 days of hydration, suggesting a more rapid pH decrease than that measured at 300 days in the present work, which resulted in a drop in the volume of H_2 released. On the other hand, three to four orders of magnitude lower volumes of H_2 (0.02 and 0.04 L/m^2) were observed in MKPC mortar (Fig. 18 left). However, the physicochemical stability of the MKPC matrix based on the M/P ratio and moisture curing condition has to be considered, as studied by Fernández-García et al. (2024). In all cases, the higher risk of H_2 release is detected in the early stages of interaction with the matrix (up to 30 days), which attenuates over time.

To confirm the attenuation process over the exposure time, the quantification of the H_2 released over 550 days of water immersion was calculated from electrochemical measurements for Al and Al–Mg alloy

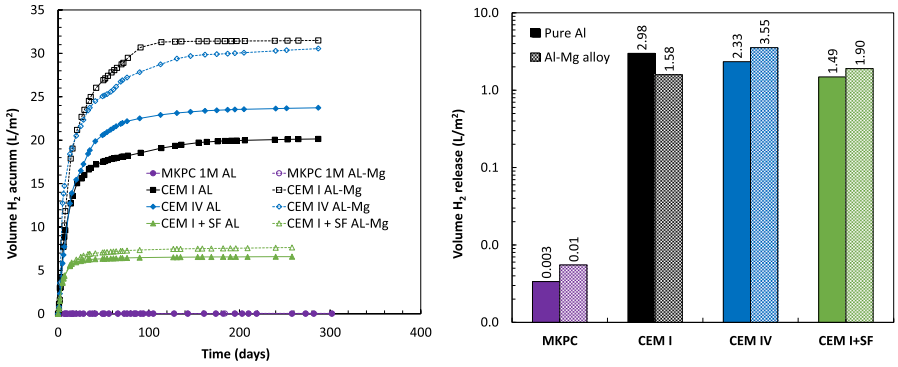

Fig. 17. Accumulated H_2 released over 300 days (left) and during the first 48 h (right) of pure Al and Al–Mg alloy in contact with MKPC, CEM I, CEM IV and CEM I+50%SF matrices immersed in water.

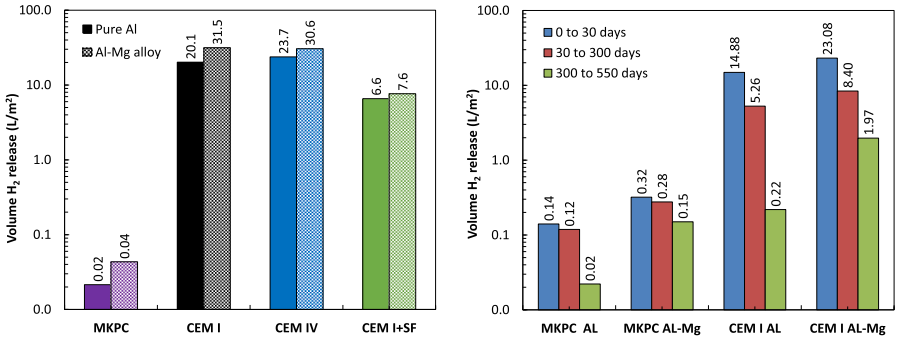

Fig. 18. Accumulated H_2 released after 300 days for MKPC, CEM I, CEM IV and CEM I+50%SF matrices (left) and H_2 evolution between 0 and 30 days, 30–300 days and 300–550 days of interaction in MKPC and CEM I mortar systems (right), for Al and Al–Mg alloy in water immersion conditions.

in MKPC and CEM I mortars. Fig. 18 right shows the accumulated H_2 released at 300 days and the increase in the 250 days of the second immersion period. A comparison with the volume released during the first 30 days of interaction is shown in Fig. 18 right and reported by Perona et al. (2023). An attenuation phenomenon is observed for both systems after 30 days of interaction, with a significant decrease and stabilisation over time. Fig. 18 right corroborates that the highest amount of H_2 is released during the first days of interaction with the matrix, as mentioned previously, with values of 0.20 and 15 L/m^2 in the MKPC and CEM I matrix, respectively. The volume of gas released is significantly reduced between 300 days and 550 days, with values of 0.08 and 1.5 L/m^2 in MKPC and CEM I matrices, respectively. The attenuation process in the H_2 released exists and depends on the interaction time with the cementitious matrix.

A comparison of H_2 released found in the literature (see Table 1) was made to identify the main discrepancies between the different studies at the exact overlapping testing times (1, 7 and 50 days) using electrochemical methods (as the chemical methods show lower H_2 values over time). Fig. 19 illustrates the comparison between the present work and literature data, representing the H_2 released using LPR and EIS techniques as a function of the pore solution pH of the different cementitious materials (MKPC, OPC type CEM I and Portland cement blended matrices). Although this representation was made using similar testing times, it shows the variability between the studies and in particular the electrochemical methods used.

Significant differences between the cement types used are detected, and a strong influence of the pore solution pH is observed. Three orders of magnitude higher values of H_2 released are found for highly alkaline CEM I and IV systems compared to more near-neutral matrices, with associated higher corrosion rates. Increasing the M/P ratio in MKPC formulation (2 and 3M) increases the pore solution pH as the phosphate content decreases, which is associated with higher values of H_2 released closer to the CEM I+50%SF matrix used in the present study. Therefore, the physicochemical stability of the MKPC matrices is a crucial factor to be considered, as reported by Fernández-García et al. (2024). The values obtained via EIS and LPR techniques appear similar during the first 24 h of interaction (Fig. 19). However, the EIS technique gives slightly higher values as time progresses. In addition, lower H_2 release is detected for Al and Al–Mg in CEM I and 1M MKPC matrices used in the present study compared to those reported in the literature at the same curing ages. Due to this, the main differences between the studies may be the use of different techniques for H_2 quantification via long-term tests and the curing condition or sample preparation.

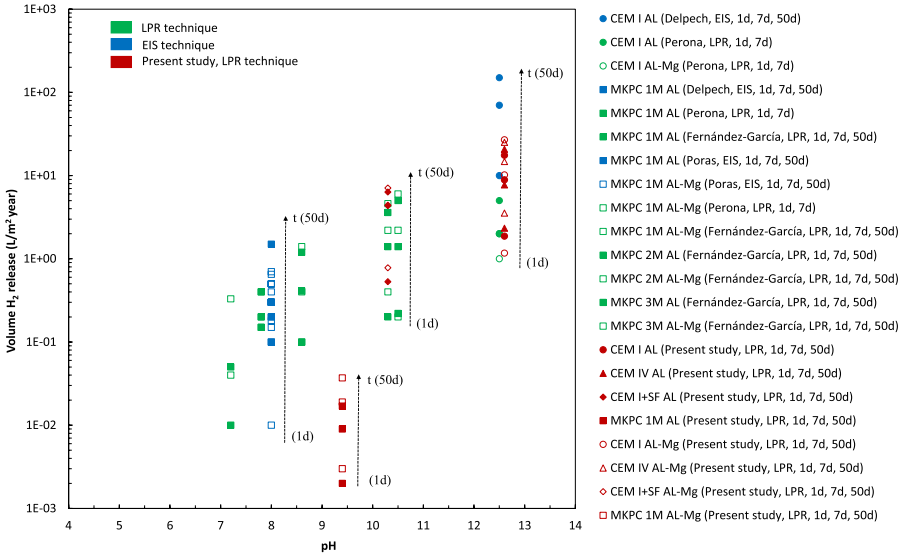

Fig. 19. H_2 production based on the literature data using electrochemical techniques in MKPC, OPC type CEM I, and Portland cement blended matrices. The results of the current study are marked in red.

5. Conclusions

Highly alkaline matrices such as OPC type CEM I and Portland blended type CEM IV show a degradation process of Al alloy with a high risk of hydrogen evolution demonstrated via LPR measurements.

In the interface between Al alloy and a CEM I matrix, a heterogeneous layer of corrosion products of aluminium and oxygen is formed with a thickness ranging from 50 to 90 μm. Al ions generated due to the high alkaline pore solution pH of CEM I can diffuse in the cement matrix. After 550 days of water immersion, an Al penetration in the matrix is detected, with aluminium content ranging from 26.1 ± 5.5% near the Al surface (≈0.8 mm) to 1.5 ± 0.3% far from the Al surface (≈7.5 mm). Al enrichment is found and reacts with the cement matrix components at 1 mm depth, forming expansive ettringite nodules.

An intense porous domain near the Al/CEM I paste interface is formed due to the high volume of H_2 release even when curing is isolated.

Expansive ettringite and a porous domain at the Al/CEM I matrix interface could affect the integrity of the waste-form in the long-term. Therefore, the use of CEM I is not recommended for Al immobilisation.

Lower corrosion rates with the lowest amounts of H_2 gas associated are detected in the 1M MKPC matrix, followed by CEM I+50%SF. A lower internal pH over time makes these matrices optimal alternatives for Al and Al–Mg alloy immobilisation compared with the commonly used CEM I system. More than two orders of magnitude difference has been found between MKPC and CEM I+50%SF matrices and the two alkaline systems, CEM I and CEM IV.

No significant metal reactivity exists with a 1M MKPC matrix interaction due to its lower pore solution pH in the Al passive domain. A protective effect of the phosphate content in the corrosion response has been identified, and a dense microlayer rich in P/Mg/K of about 30 μm at the Al surface is observed. No region with higher porosity has been found at the Al/MKPC matrix transition zone due to lower Al reactivity and a lower amount of H_2 released.

CRediT authorship contribution statement

C. Fernández-García: Writing – original draft, Methodology, Investigation, Formal analysis. **P. Padilla-Encinas:** Writing – original draft, Methodology, Investigation, Formal analysis. **R. Fernández:** Writing – review & editing, Validation, Supervision, Investigation, Conceptualization. **M.C. Alonso:** Writing – review & editing, Validation, Supervision, Investigation, Conceptualization.

Declaration of competing interest

The authors declare that they have no known competing financial interests or personal relationships that could have appeared to influence the work reported in this paper.

Data availability

Data will be made available on request.

Acknowledgments

The authors acknowledge the Project funding from the European Union's Horizon 2020 Research and Innovation Program for Nuclear Fission and Radiation Protection Research (call NFRP-2019-2020) under grant agreement No. 945098 (PREDIS). Also acknowledge of C.F.G and M.C.A. for the project funded by CSIC, PIE No. 202260E009.

References

Alonso, M.C., García-Calvo, J.L., Petterson, S., Cuñado, M.A., Vuorio, M., Weber, H., Ueda, H., Naito, H., 2012. AB R-12-02 Development of an Accurate pH Measurement Methodology for the Pore Fluids of Low pH Cementitious Materials.

Andrade, C., Alonso, C., 2004. Test methods for on-site corrosion rate measurement of steel reinforcement in concrete by means of the polarization resistance method. Mater. Struct. 37, 623–643. https://doi.org/10.1007/BF02483292.

ASTM-G102-89, 1999. Standard Practice for Calculation of Corrosion Rates and Related Information from Electrochemical Measurements.

Caes, S., Gurning, A.C., Li, X., de Souza, V., Kursten, B., 2023. Corrosion of aluminium in ordinary Portland cement paste: influence of matrix porosity and the presence of LiNO3 corrosion inhibitor. Mater. Corros. 74, 125–137. https://doi.org/10.1002/maco.202213296.

Cau Dit Coumes, C., Lambertin, D., Lahalle, H., Antonucci, P., Cannes, C., Delpech, S., 2014. Selection of a mineral binder with potentialities for the stabilization/solidification of aluminum metal. J. Nucl. Mater. 453, 31–40. https://doi.org/10.1016/j.jnucmat.2014.06.032.

Certificación, A.E. de N. y, 1996. UNE-EN 196-1:1996: métodos de ensayo de cementos : parte 1: determinación de resistencias mecánicas. Asociación Española de Normalización y Certificación.

Chong, L., Yang, J., Shi, C., 2017. Effect of curing regime on water resistance of magnesium–potassium phosphate cement. Construct. Build. Mater. 151, 43–51. https://doi.org/10.1016/j.conbuildmat.2017.06.056.

Collier, N.C., Milestone, N.B., Swift, P.D., 2010. Immobilisation matrices for intermediate level nuclear wastes using sulphate activated BFS/OPC and PFA/OPC composite cements. Adv. Appl. Ceram. 109, 269–274. https://doi.org/10.1179/174367509X12447975734276.

Covill, A., Hyatt, N.C., Hill, J., Collier, N.C., 2011. Development of magnesium phosphate cements for encapsulation of radioactive waste. Adv. Appl. Ceram. 110, 151–156.

Delpech, S., Cannes, C., Barré, N., Tran, Q.T., Sanchez, C., Lahalle, H., Lambertin, D., Gauffinet, S., Coumes, C.C.D., 2017. Kinetic model of aluminum behavior in cement-based matrices analyzed by impedance spectroscopy. J. Electrochem. Soc. 164, C717–C727. https://doi.org/10.1149/2.0211713jes.

Deshwal, G.Kr, Panjagari, N.R., 2020. Review on metal packaging: materials, forms, food applications, safety and recyclability. J. Food Sci. Technol. 57, 2377–2392. https://doi.org/10.1007/s13197-019-04172-z.

Diamond, S., 1996. Delayed ettringite formation — processes and problems. Cem. Concr. Compos. 18, 205–215. https://doi.org/10.1016/0958-9465(96)00017-0.

Diaz Caselles, L., Cau Dit Coumes, C., Antonucci, P., Rousselet, A., Mesbah, A., Montouillout, V., 2024a. Leaching of magnesium potassium phosphate cement pastes under alkaline conditions. Appl. Geochem. 170, 106067 https://doi.org/10.1016/j.apgeochem.2024.106067.

Diaz Caselles, L., Cau Dit Coumes, C., Antonucci, P., Rousselet, A., Mesbah, A., Montouillout, V., 2024b. Chemical degradation of magnesium potassium phosphate cement pastes during leaching by demineralized water: experimental investigation and modeling. Cement Concr. Res. 178, 107456 https://doi.org/10.1016/J.CEMCONRES.2024.107456.

Fernández-García, C., Cruz Alonso, M., María Bastidas, J., García-Lodeiro, I., Fernández, R., 2024. MgO/KH2PO4 and curing moisture content in MKPC matrices 2 to optimize the immobilization of pure Al and Al-Mg alloys. Materials 17, 1263. https://doi.org/10.3390/ma17061263.

García Calvo, J.L., Alonso, M.C., Hidalgo, A., Fernández Luco, L., Flor-Laguna, V., 2013. Development of low-pH cementitious materials based on CAC for HLW repositories: long-term hydration and resistance against groundwater aggression. Cement Concr. Res. 51, 67–77. https://doi.org/10.1016/J.CEMCONRES.2013.04.008.

García Calvo, J.L., Hidalgo, A., Alonso, C., Fernández Luco, L., 2010. Development of low-pH cementitious materials for HLRW repositories: resistance against ground waters aggression. Cement Concr. Res. 40, 1290–1297. https://doi.org/10.1016/J.CEMCONRES.2009.11.008.

Gardner, L.J., Corkhill, C.L., Walling, S.A., Vigor, J.E., Murray, C.A., Tang, C.C., Provis, J. L., Hyatt, N.C., 2021. Early age hydration and application of blended magnesium potassium phosphate cements for reduced corrosion of reactive metals. Cement Concr. Res. 143 https://doi.org/10.1016/j.cemconres.2021.106375.

Hayes, M., Godfrey, I.H., 2007. Development of the use of alternative cements for the treatment of intermediate level waste. In: Proc. Conf. WM, vol. 7.

Ionascu, L., Nicu, M., Turcanu, C., Dragolici, F., Rotarescu, G.H., 2014. Study of the conditioning matrices for aluminium radioactive wastes. Rom. J. Phys. 59, 360–368.

Kinoshita, H., Swift, P., Utton, C., Carro-Mateo, B., Marchand, G., Collier, N., Milestone, N., 2013. Corrosion of aluminium metal in OPC- and CAC-based cement matrices. Cement Concr. Res. 50, 11–18. https://doi.org/10.1016/j.cemconres.2013.03.016.

Kónya, J., Nagy, N.M., 2018. Chapter 7: Nuclear Energy Production in Nuclear and Radiochemistry, second ed. Elsevier.

Krall, L.M., Macfarlane, A.M., Ewing, R.C., 2022. Nuclear waste from small modular reactors. Proc. Natl. Acad. Sci. USA 119, e2111833119. https://doi.org/10.1073/pnas.2111833119.

Liu, S., Chang, S., Tu, Y., Luo, S., 2023. Immobilisation mechanism for nuclear waste containing aluminium by supersulfated cement containing phosphogypsum. Cem. Concr. Compos. 139 https://doi.org/10.1016/j.cemconcomp.2023.104991.

Mendibide, C., Dusquesnes, V., Deydier, V., Bourbon, X., Crusset, D., 2021. Corrosion behavior of aluminum alloy 5754 in cement-based matrix-simulating nuclear waste disposal conditions. Mater. Corros. 72, 383–395. https://doi.org/10.1002/maco.202011687.

Nygaard, P.V., Geiker, M.R., Elsener, B., 2009. Corrosion rate of steel in concrete: evaluation of confinement techniques for on-site corrosion rate measurements. Mater. Struct. 42, 1059–1076. https://doi.org/10.1617/s11527-008-9443-1.

Padilla-Encinas, P., Dieguez, M., Cuevas, J., Ruiz, A.I., Fernández, R., 2024. The influence of the magnesium-to-phosphate molar ratio on magnesium potassium phosphate cement properties using either wollastonite or volcanic ash as fillers. Minerals 14, 103. https://doi.org/10.3390/min14010103.

Pandey, S.P., Sharma, R.L., 2000. The influence of mineral additives on the strength and porosity of OPC mortar. Cement Concr. Res. 30, 19–23. https://doi.org/10.1016/S0008-8846(99)00180-5.

Paraskevoulakos, C., Stitt, C.A., Hallam, K.R., Banos, A., Leal Olloqui, M., Jones, C.P., Griffiths, G., Adamska, A.M., Jowsey, J., Scott, T.B., 2019. Monitoring the degradation of nuclear waste packages induced by interior metallic corrosion using synchrotron X-ray tomography. Construct. Build. Mater. 215, 90–103. https://doi.org/10.1016/J.CONBUILDMAT.2019.04.178.

Perona, R., Fernández-García, C., García-Lodeiro, I., Criado, M., Bastidas, J.M., Alonso, M.C., 2023. Corrosion behavior and immobilization of pure aluminum and Al−Mg alloy LLRW in magnesium potassium phosphate cements. J. Nucl. Mater. 582, 154501 https://doi.org/10.1016/j.jnucmat.2023.154501.

Poras, G., Cau Dit Coumes, C., Antonucci, P., Cannes, C., Delpech, S., Perrin, S., 2023. Electrochemical behavior of Al/Mg alloys immobilized in a magnesium potassium phosphate cement-based mortar. Materials 16. https://doi.org/10.3390/ma16155415.

Pourbaix, M., Burbank, J., 1964. Atlas D-equilibres electrochimiques. J. Electrochem. Soc. 111, 14C. https://doi.org/10.1149/1.2426051.

Rahman, R.O.A., Rakhimov, R.Z., Rakhimova, N.R., Ojovan, M.I., 2014. Alternative binders. In: Cementitious Materials for Nuclear Waste Immobilization. John Wiley & Sons, Ltd, pp. 79–104. https://doi.org/10.1002/9781118511992.ch4.

Setiadi, A., Milestone, N.B., Hill, J., Hayes, M., 2006. Corrosion of aluminium and magnesium in BFS composite cements. Adv. Appl. Ceram. 105, 191–196.

Sharma, R.L., Pandey, S.P., 1999. Influence of mineral additives on the hydration characteristics of ordinary Portland cement. Cement Concr. Res. 29, 1525–1529. https://doi.org/10.1016/S0008-8846(99)00104-0.

Stern, M., Geary, A.L., 1957. Electrochemical polarization I. A theoretical analysis of the shape of polarization curves. J. Electrochem. Soc. 104, 56–63.

Vargel, C., 2020. Corrosion of Aluminium. Elsevier.

Vollpracht, A., Lothenbach, B., Snellings, R., Haufe, J., 2016. The pore solution of blended cements: a review. Mater. Struct. 49, 3341–3367. https://doi.org/10.1617/s11527-015-0724-1.

Wang, X., Hu, X., Yang, J., Chong, L., Shi, C., 2022. Research progress on interfacial bonding between magnesium phosphate cement and steel: a review. Construct. Build. Mater. 342, 127925.

Won, K., Han, J., Bonne, A., 1997. Radioactive waste disposal: global experience and challenges. IAEA Bull. 39, 33–41.

Zhou, Q., Milestone, N.B., Hayes, M., 2006. An alternative to Portland Cement for waste encapsulation—the calcium sulfoaluminate cement system. J. Hazard Mater. 136, 120–129. https://doi.org/10.1016/J.JHAZMAT.2005.11.038.